INTERNATIONAL JOURNAL OF CLIMATOLOGY
Int. J. Climatol. **18**: 1521–1537 (1998)

SEASONAL MODULATED INTRASEASONAL OSCILLATIONS IN A GCM SIMULATION

JIAN-PING HUANG[a,*] and HAN-RU CHO[b]
[a] *ARQM/AES, Environment Canada, Downsview, Ontario, M3H ST4, Canada*
[b] *Department of Physics, University of Toronto, Toronto, Ontario, M5S 1AT, Canada*

Received 4 June 1997
Revised 12 March 1998
Accepted 6 April 1998

ABSTRACT

The seasonal variation of intraseasonal oscillations have been studied on a zonally symmetric all-land planet in the absence of external forcing, using the second version of the NCAR community climate model (CCM2, R15). Analysis of both 15-year perpetual and seasonal simulations indicates the seasonal cycle strongly modulates the intraseasonal oscillations. The averaged period of oscillation in seasonal simulation is 50 days, while it is 40 days in the perpetual run. It also has larger amplitudes during the winter than during the summer. Statistics of phase variation show that the probability distribution of phase changes has also an obvious seasonal variation, especially in the mid-latitudes, where the probability distribution is narrow centered 40–50 days in period in the winter hemisphere, but is broad in the summer hemisphere. © 1998 Royal Meteorological Society.

KEY WORDS: seasonal variation; intraseasonal oscillation; cyclic spectral analysis; CCM2 simulation

1. INTRODUCTION

Oscillations of the atmosphere are determined by complex interactions between its internal dynamics and slowly changing external forcing (such as sea surface temperature, soil moisture, sea ice, snow, and solar radiation, etc). Among the problems not yet well understood is how the seasonal cycle modulates the 30–60-day oscillation. The oscillation was first discovered by Madden and Julian (1971), Madden and Julian, 1972), and is also referred to as the intraseasonal oscillation in the literature. Recent observational studies indicate that its amplitudes are seasonally dependent. Although they occur throughout the year without any systematic change in periodicity (Anderson and Rosen, 1983), the locations of maximum OLR variability and the extratropical response to their occurrence do exhibit seasonality (Knutson and Weickmann, 1987). Madden (1986) found that the intraseasonal oscillations exhibit seasonal variations, in both intensity and phase speed. Oscillations are strongest during December–February and weakest during June–August. Gutzler and Madden (1993) showed that the intraseasonal oscillations in the global momentum are strongest in the late winter and weakest in the fall. Annual variation of sea surface temperature, wind and convection have been recognized as the primary climatological factors determining the annual variability of the intraseasonal oscillation (Madden, 1986; Gutzler and Madden, 1993; Wang and Rui, 1990). There are also other possible but yet unidentified effects due to the season.

This study attempts to explore these yet unidentified effects. Although the observed intraseasonal oscillation is extremely episodic and exhibits large interannual variation, this paper only focuses on the study of its seasonal variation. The approach is to generate an artificial climate with a commonly used general circulation model (GCM) of the atmosphere, instead of using observational data. Many essential

* Correspondence to: ARQM/AES, Environment Canada, Downsview, Ontario, M3H ST4, Canada;
e-mail: Jianping.Huang@ec.gc.ca

Contract grant sponsor: Canadian Natural Science and Engineering Council, the Atmospheric Environment Service of Canada

CCC 0899–8418/98/141521–17$17.50

features of intraseasonal oscillation are reproducible in various versions of atmospheric general circulation models (GCMs). The success of an aqua-planet GCM (Hayashi and Sumi, 1986; Yip and North, 1993) and GCMs with axially symmetric climatology (Hayashi and Golder, 1986; Lau and Lau, 1986) in simulating intraseasonal oscillations indicates that neither land–sea thermal contrasts nor zonal asymmetry is necessary to explain the existence of the oscillation. To identify the effects of the seasons and to examine their physical causes, efforts are made to keep the model as simple as possible without the complications of many unnecessary factors such as land–sea asymmetry of the atmosphere–ocean system, and the topographic forcing of the atmosphere, etc. The results from such a model are of course not as realistic when compared with other GCMs, but it is easier to interpret and to identify the physical causes for the seasonal effects in intraseasonal oscillations.

The model used in this paper is the NCAR community climate model version 2 (CCM2) with rhomboidal truncation at zonal wave number 15 (R15). As explained in the previous paragraph, the ocean and the topography are removed from the model. The soil moisture and vegetation are prescribed to be 75% saturated and shrubland (type 5), respectively. Such an idealized GCM with zonally symmetric climate provides a simple environment for the intraseasonal oscillations to develop (Yip and North, 1993; Huang and North 1996; Huang *et al*., 1996). The motivation of using a land-only model is that this model removes the effective 5-year relaxation time of the mixed-layer ocean. The seasonal variation of solar radiation is the only time dependent forcing. For the purpose of comparison, we have conducted 15-year simulations with and without seasons. The daily average solar radiation was used as the solar heating rate. In the perpetual simulation, the obliquity (tilt angle of planetary spin axis with respect to the normal of orbital plane) of the planet was set to zero so that the model is run in an equinox solar insolation regime perpetually. In the seasonal simulation, the declination angle will vary from $-11.74°$ to $11.75°$ over 1 year (half the range for earth). A weaker seasonal forcing is used to prevent an excessive seasonal cycle on an all land planet. No interannual variability will be introduced to the external forcing of the model. The primary goal of this paper is to compare the behavior and identify the differences of intraseasonal oscillations between these two simulations.

Due to the forcing of the seasonal cycle, the climate system is not stationary in time. It has been pointed out by Huang and North (1996) and Huang *et al.* (1996) that traditional methods related to Fourier spectral decomposition are inappropriate in an analysis of non-stationary time series. Madden (1986) has developed a seasonally varying cross-spectral analysis technique. This important technique, however, is based on the assumption of stationarity. The present paper attempts to employ newly developed cyclic spectral analysis to study the seasonal variation of intraseasonal oscillations in these specific GCM simulations. Before the analysis of the CCM2 simulated data, it is necessary to review cyclic spectral analysis and illustrate some applications on analytic seasonally modulated oscillations, as per section 2. Section 3 applies cyclic spectral analysis to the simulated oscillation. Section 4 gives the composite structure. Finally, the main results are summarized in section 5.

2. CYCLIC SPECTRAL ANALYSIS

Analogous to the dual time- and frequency-domains for stationary processes one can define the seasonally varying spectral density as

$$S(t,f) = \sum_{\alpha} S^{\alpha}(f)\, \mathrm{e}^{i2\tau\alpha t}, \tag{1}$$

where t is the time, f the frequency, S^{α}, the cyclic spectral density and α is the cycle frequency. The seasonally varying cross-spectral density S_{12} and cyclic cross-spectra S_{12}^{α} for two cyclostationary signals $T_1(t)$ and $T_2(t)$ are given by

$$S_{12}(t,f) = \sum_{\alpha} S_{12}^{\alpha}(f)\, \mathrm{e}^{i2\pi\alpha t} \tag{2}$$

and

$$S_{12}^{\alpha}(f) = \int_{-\infty}^{+\infty} C_{12}^{\alpha}(\tau)\, \mathrm{e}^{-i2\pi f\tau}\, \mathrm{d}\tau, \tag{3}$$

where $C_{12}^{\alpha}(\tau)$ is said to be a cyclic cross-covariance at cycle frequency α. The seasonally varying coherence squared and phase are thus

$$\mathrm{Coh}^2(t,f) = \frac{P_{12}(t,f)^2 + Q_{12}(t,f)^2}{S_1(t,f)S_2(t,f)} \tag{4}$$

$$\theta_{12}(t,f) = \tan^{-1}\frac{Q_{12}(t,f)}{P_{12}(t,f)}, \tag{5}$$

where the $P_{12}(t,f)$ and $Q_{12}(t,f)$ are the real and imaginary parts of the cross spectrum, respectively. $S_1(t,f)$ and $S_2(t,f)$ are the seasonally varying spectra for $T_1(t)$ and $T_2(t)$. A comprehensive treatment of cyclic spectral analysis can be found in Gardner (1994), Huang and North (1996) and Huang *et al.* (1996), and references therein.

Before the analysis of the CCM2 simulated oscillation, the cyclic spectral analysis is illustrated for two analytic seasonally modulated 40-day oscillations. A one-dimensional analytical oscillation in a climatic system is generally depicted as

$$X(t) = A(\tau)\cos(2\pi f_0 t + \Phi(\tau)), \tag{6}$$

where f_0 is the fundamental frequency of oscillation, $A(\tau)$ and $\Phi(\tau)$ are the amplitude and phase which vary on a slow time scale τ, respectively. If both the amplitude and phase remain unchanged with time, (i.e. $A(\tau) = A_0$, $\Phi(\tau) = \Phi_0$), the oscillation is stationary in time and its seasonally varying spectra (not shown) is represented by a straight line centered at frequency f_0. For an amplitude-modulated oscillation, the phase does not change with time (i.e. $\Phi(\tau) = \Phi_0$), but the amplitude is modulated by a lower-frequency oscillation, such as the seasonal cycle, (i.e. $A(\tau) = A_0\cos(2\pi f_m\tau)$, where f_m is the frequency of modulation). In this case, the seasonally varying spectra (Figure 1(a)) exhibits two prominent characteristics: (i) a periodic waveform in the time domain which corresponds to amplitude modulation; and (ii) the dominant frequency appearing as a horizontal line centered at frequency f_0 which reflects the constancy of the fundamental periodicity in time. The amplitude modulated fluctuation is often found in a climate system involving nonlinear interaction between different scales or interference of a frequency component from its sidebands.

For a frequency modulated oscillation ($A(\tau) = A_0$, $\Phi(\tau) = \Phi_0\sin(2\pi f_m\tau)$), the major characteristic is that the dominant frequency changes with time in the period at frequency of modulation. The periodic variation of frequency shows up clearly in the seasonally varying spectra (Figure 1(b)). The frequency modulated oscillation is often associated with the physical property changes in the climate system, such as the variation of atmospheric moisture due to the seasonal cycle. This may change the stability of the atmosphere and alter the frequency of its normal modes (Lau and Weng, 1995; Huang *et al.*, 1997).

3. ANALYSIS OF CCM2 SIMULATED OSCILLATION

Both 15-year perpetual and seasonal simulations have been conducted and the outputs are analyzed in this section. To facilitate the comparison between seasonal and perpetual simulations, the usual practice is to remove the seasonal cycle from the data of the seasonal simulation prior to the spectral analysis, by using the normalization

$$x' = \frac{x - \bar{x}}{\sigma(x)}, \tag{7}$$

where x is the daily data, $\bar{x}$ is a seasonally varying mean and $\sigma(x)$ is a S.D. calculated according to

$$\sigma(x) = \sqrt{\sum_{k=1}^{K} (x - \bar{x})^2/(K-1)}, \tag{8}$$

where k is an index indicating the number of the data, and K is the total number. It is often assumed that the oscillations are linearly superimposed on the seasonal cycle and the seasonal cycle can be 'removed' by simply using the normalization procedure. If this is the case, the spectrum of x' in a seasonal simulation should be similar to that in a perpetual run. Huang *et al.* (1996) has shown that the 'seasonal cycle' cannot be completely 'removed' by using the procedure outlined in Equations (7) and (8). In the next subsection, the space–time spectral analysis is made using x' of both the perpetual and seasonal simulations. A cyclic spectral analysis will be made for the seasonal simulation data in subsection 3.2.

3.1. Space–time spectral analysis

The total variance and the contribution of different wave components to the total variance of zonal wind at 189 hPa is calculated. Wave number one contributes the most (43%) to the total variance, and wave number two contributes about 20%. The spectral analysis of only wave number one, therefore, will be presented in this section.

To detect the presence of intraseasonal oscillation in this simplified model atmosphere, the space–time spectral analysis technique developed by Hayashi (1982) will be used in this subsection. Figure 2 displays the space–time power spectral density of 189 hPa zonal winds of the seasonal and perpetual runs for wave number one at four latitudes. The solid line represents the spectral density of the seasonal run, while the dashed line represents the perpetual simulation. Figure 3 shows analogous plots for the 189 hPa meridional wind. A conspicuous spectral peak with a period of 40–50 days occurs in both the perpetual

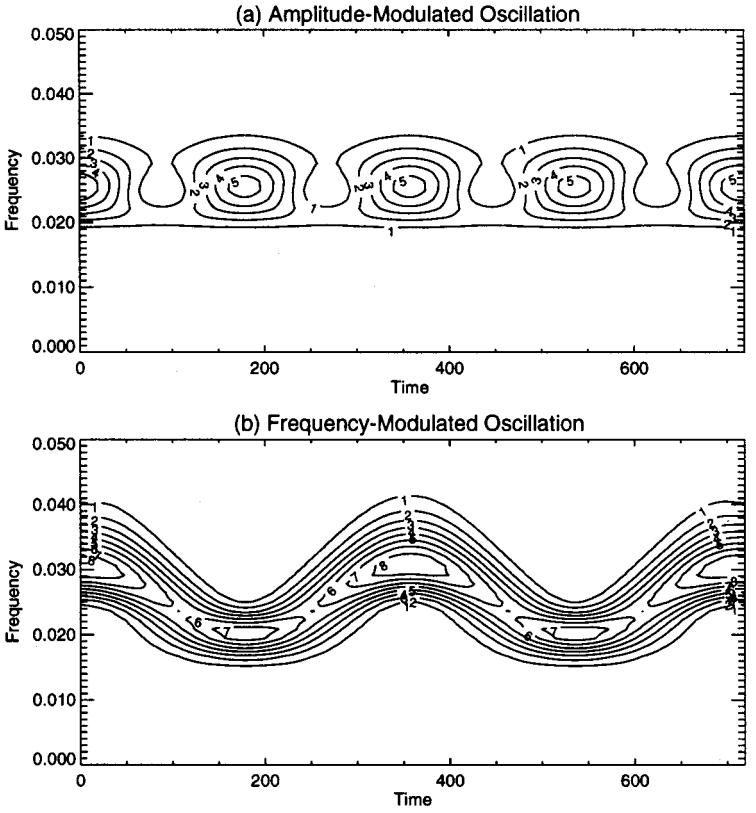

Figure 1. Seasonally varying spectra of the analytic modulated oscillations: (a) amplitude-modulated oscillation; (b) frequency-modulated oscillation. The fundamental frequency is $f_0 = 0.025$ (40 days); the modulated frequency is $f_m = 0.0028$ (360 days). Contour interval is 1.0

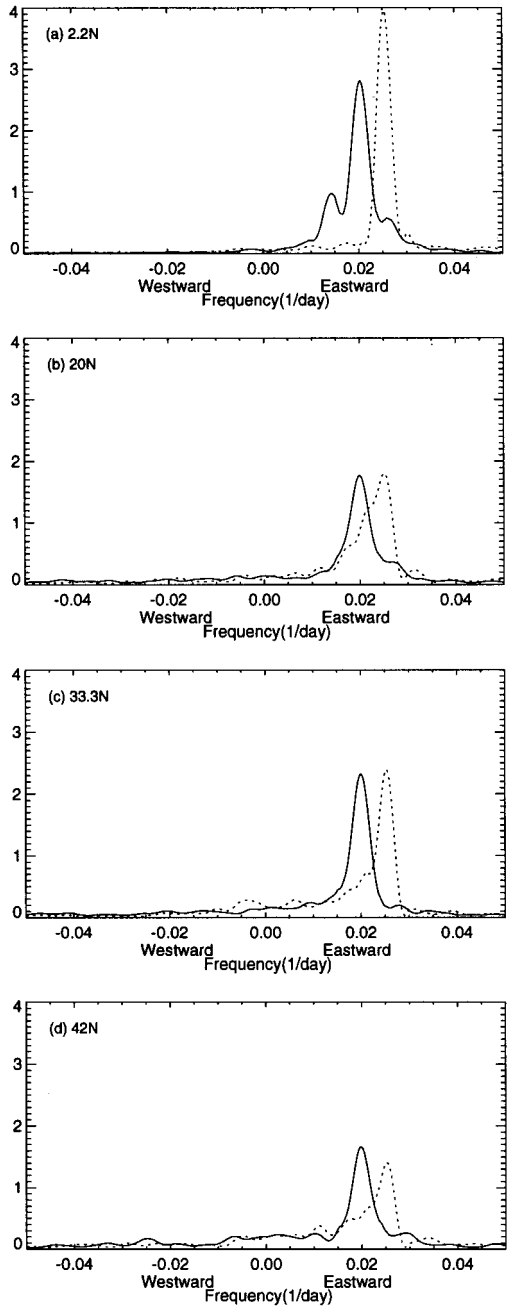

Figure 2. The standardized space–time power spectral density of the 189 hPa zonal wind for wave number one at (a) 2.2°N; (b) 20°N; (c) 33.3°N; (d) 42°N. The solid line represents the spectral density of seasonal run, while the dash line represents the perpetual run

and seasonal runs. These spectral peaks represent waves which propagate eastward, and take *ca.* 40–50 days to encircle the globe. The oscillation period in either the seasonal or the perpetual simulations is significantly longer than those in most of the other GCM results (Hayashi and Sumi 1986; Lau and Lau 1986; Pitcher and Geisler 1987; Lau *et al.* 1988). Unlike the GFDL (Hayashi and Golder, 1993) simulation, there is no 25–30-day spectral peak in the wave number one component.

A significant difference between the seasonal and perpetual simulation is in the locations of the peaks, i.e. it is located at about 40 days in the perpetual run and 50 days for the seasonal run at all latitudes in both zonal and meridional wind fields. Another interesting feature to note in Figures 2 and 3 is that the relative intensities of the peaks of these two figures vary with latitude.

The space–time spectra, however, show no information regarding their seasonal locality since the spectra are averages of the entire data record. Cyclic spectral analysis was suggested as a substitute for analysis of oscillations that exhibit a seasonal variation. This technique is applied in order to study the seasonal variation of the intraseasonal oscillation in the seasonal simulation in the following subsection.

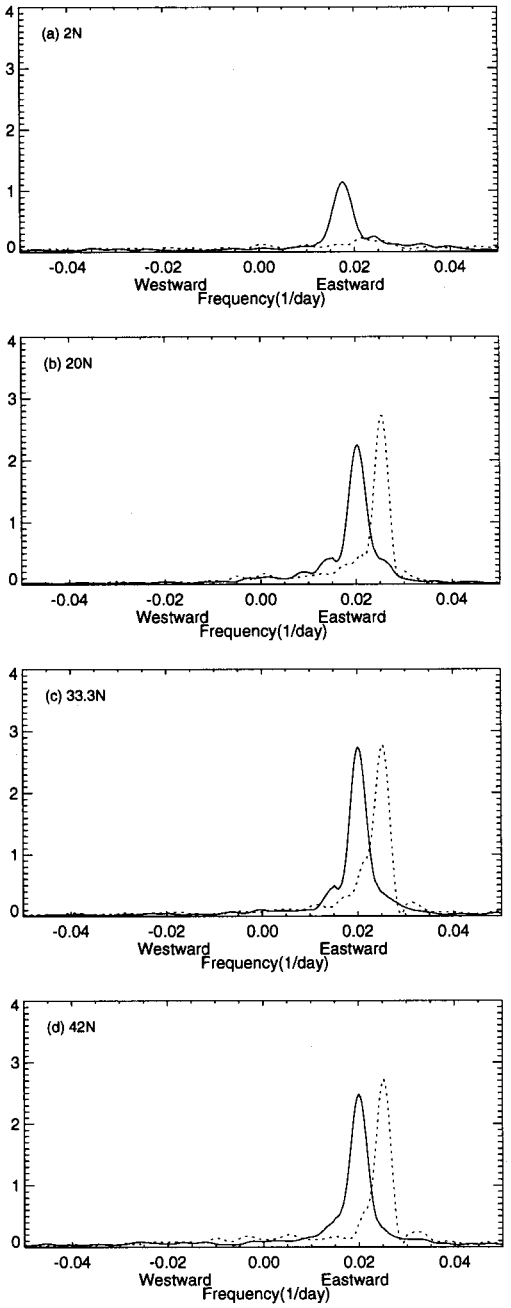

Figure 3. As in Figure 2 but for meridional wind

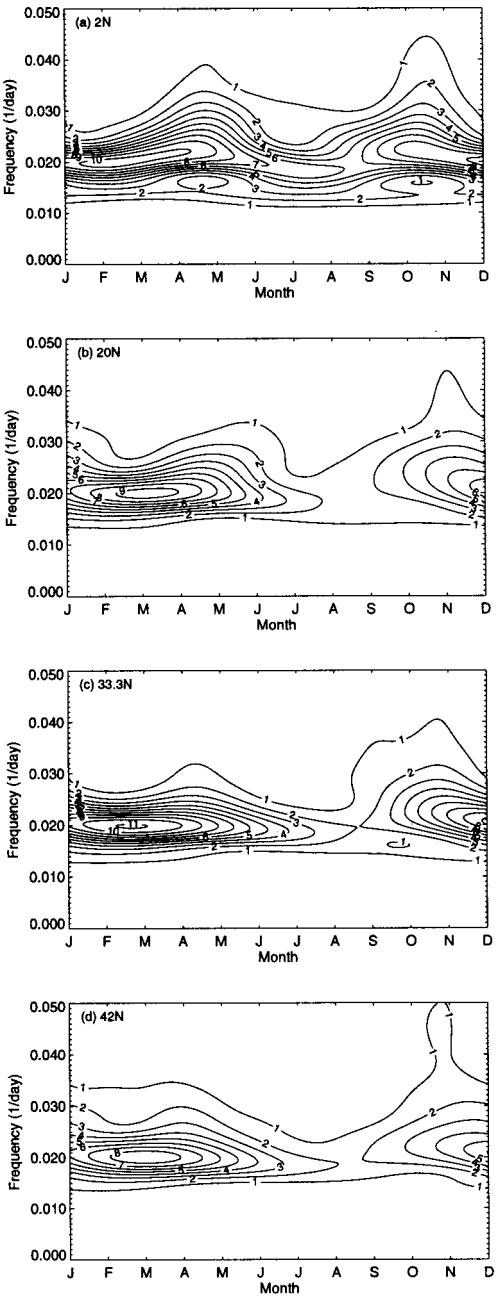

Figure 4. Seasonal variation of spectra of eastward moving wave number one for 189 hPa zonal wind at (a) 2.2°N; (b) 20°N; (c) 33.3°N; (d) 42°N

3.2. Cyclic spectral analysis

Figure 4 shows the seasonal variations of spectra of eastward-moving wave number one for the 189 hPa zonal wind at four latitudes. There are obvious oscillations at 50-day periods whose amplitudes show significant seasonal variations. A seasonal maximum in late-winter and early-spring at all latitudes is an ubiquitous feature in all panels. Figure 4 suggests that the nearly 50-day spectral peak in Figure 2(b–d) is primarily associated with fluctuations during winter and spring. Figure 5 shows the same as in Figure

4 but for 993 hPa. At mid-latitudes, the spectral peaks of the lower levels are much weaker than those in the upper levels throughout the year.

Figure 6 shows the seasonal variation of coherence square and the phase difference between 189 and 993 hPa levels for eastward-moving wave number one of zonal wind at the 50-day frequency band, at 2.2°N. The band width is 0.018–0.022 (1/day). The upper and lower level intraseasonal disturbances are coherent at the 50-day frequency band throughout the year. The seasonal maximum coherence squares exceed 0.5 in February. The phase difference shows the 993 hPa disturbance is 172° out of phase with the

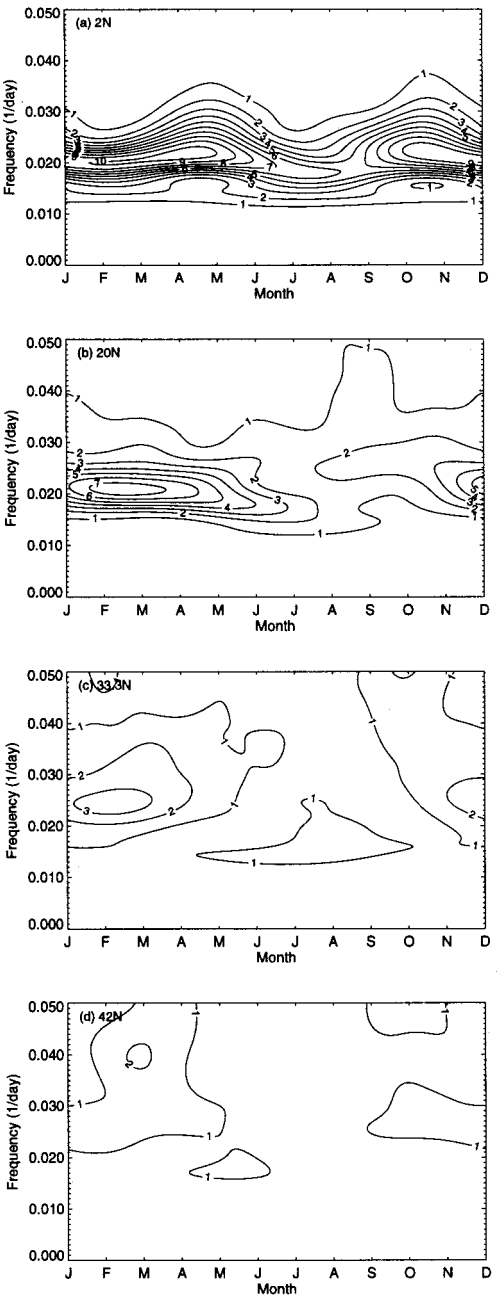

Figure 5. As in Figure 4 but for 993 hPa

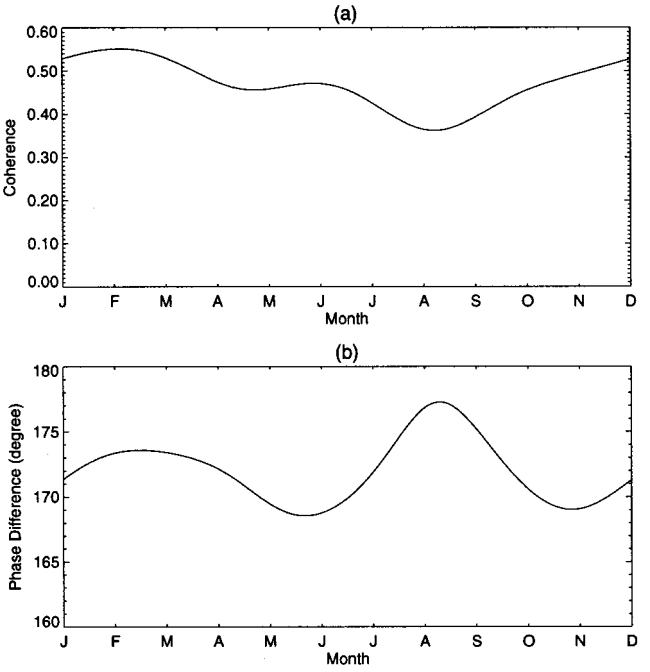

Figure 6. Seasonal variation of coherence squared and phase difference of eastward moving wave number one between 189 hPa and 993 hPa zonal wind at 50-day frequency band at 2.2°N

189 hPa one. Despite the phase difference changes with season, there is no clear trend from winter to summer. It is consistent with that found in observational studies (e.g. Madden 1986). It has been shown theoretically that the response of the tropical atmosphere to latent heating is about 180° out of phase between lower-and upper-tropospheric zonal winds. Furthermore, it is well established that cloudiness, presumably convection and the attendant tropospheric heating, is associated with intraseasonal oscillations.

In earlier studies (Madden and Julian 1971, 1972), no peaks were found in the meridional wind spectra as pronounced as those in the zonal wind spectra at 40–50-day periods. On the other hand, both theoretical and simulation studies indicate that convective forcing near the equator, which is presumed to be important in the 40–50-day oscillation, excites Rossby waves as well as Kelvin waves. The Rossby waves have meridional wind perturbations of comparable magnitude to that of the zonal wind perturbation (Yip and North 1993). These results prompted the computation of seasonally varying spectra for meridional wind and cross-spectra between zonal wind and meridional wind, to see if they could shed more light on the role of the meridional wind.

In contrast to the zonal wind, there is only a weak spectral peak of the meridional wind near the equator, (Figure 7(a)) which shows marked seasonal variation. Away from the equator, however, the spectral peak becomes quite strong (Figure 7(b–d)). A similar analysis of the 993 hPa meridional wind leads to a similar conclusion (Figure 8), except that spectral peaks are reduced at middle and high latitudes (Figure 8(d)). Figure 9 shows the seasonal variation of coherence square and phase difference between zonal wind and meridional wind of the eastward moving wave number one at 189 hPa. The coherence exhibits significant seasonal changes at all latitudes. Maximum values of coherence are obtained during the months when the values of spectra are highest, and minimum values occur in summer when the values of spectra are low. Another interesting feature to note in Figure 9 are the phase relations at these latitudes. In the tropics, the two variables are nearly over 100° out of phase, while in mid-latitudes they are nearly in phase. These results further confirm that the intraseasonal oscillation is associated with a horizontally coupled Rossby-Kelvin wave. The out of phase relation between zonal and meridional

winds in the tropics results from the variation of cross-equatorial flow from the summer to the winter hemisphere (Madden, 1986).

3.3. Statistics of phase variation

To examine whether the low-frequency wave has a preferred phase speed and propagation direction, the phase variation of wave number one, in both perpetual and seasonal simulations, is studied. The phase of

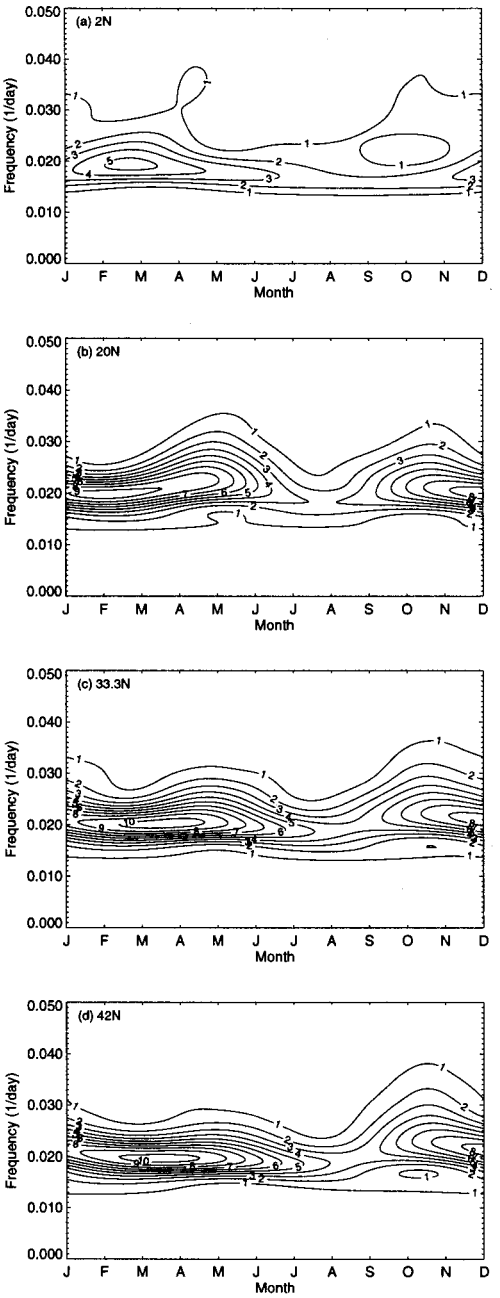

Figure 7. Seasonal variation of spectra of eastward moving wave number one for 189 hPa meridional wind at (a) 2.2°N; (b) 20°N; (c) 33.3°N; (d) 42°N

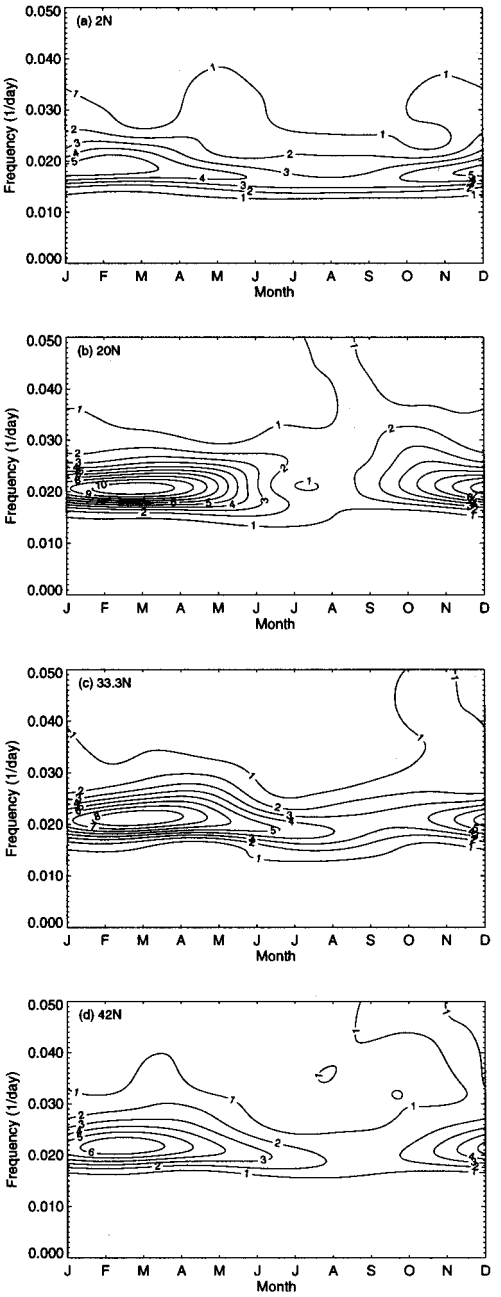

Figure 8. As in Figure 7 but for 993 hPa

the wave portion of a low-frequency flow $S(\lambda, \phi, p, t)$ can be obtained by performing a Fourier analysis in the zonal direction. The phase change during a day, $\Delta\Theta(t)$, is defined as

$$\Delta\Theta(t) = -(\Theta(\phi_0, p_0, t) - \Theta(\phi_0, p_0, t - \Delta t)) \tag{9}$$

with $\Delta t = 1$ day. Here $\Theta(\phi, p, t)$ is the phase angle of the wave at the latitude ϕ, level p and time t. A positive (negative) $\Delta\Theta(t)$ means an eastward (westward) propagation of the low-frequency wave.

Shown in Figure 10 are the normalized probability functions of $\Delta\Theta(t)$ for 189 hPa zonal wind of wave number one at four latitudes in the perpetual simulation. The most striking feature in all of the four latitudes is that the probability of an eastward propagation is remarkably large. The probability functions all have a narrow-band distribution, indicating a steady movement of the waves. The occurrence probability of eastward-moving waves within a period of 40–50 days is 28% at the equator, and 24% in the mid-latitudes. The occurrence probability of the same within a period of 20–25 days is 27% at the equator, and 15–20% in the mid-latitudes. The probability of quasi-stationary waves (i.e. the phase change is zero) is more than 15% in all latitudes. The averaged period is 40 days.

Figure 11 presents the histogram of daily phase changes during December–January–February (DJF) in the seasonal simulation. The probability in the northern hemisphere with period of 40–50 days is about 55%. Comparing the probability of the phase change in the winter hemisphere (Figure 11(a, b)) with that of the summer hemisphere (Figure 11(c, d)), an obvious seasonal variation becomes apparent, especially in the mid-latitudes, where the probability distribution is very broad during summer. The probability in the southern hemisphere with a period of 40–50 days is reduced to 45% at the equator (Figure 11(c)) and 22% in the mid-latitudes (Figure 11(d)). Another difference is that during the summer more than 25% of the low-frequency waves move westward in the mid-latitudes. The oscillation is more clearly defined in the winter than in the summer, especially at mid-latitudes.

4. COMPOSITE STRUCTURE

The composite structure will be presented in this section in order to clarify and extend the interpretations of the cyclic spectra. Since all boundary conditions are zonally symmetric, stationary waves do not appear in the present model atmosphere. If one travels in a frame moving with the phase speed of a wave, then the traveling wave becomes 'stationary' in this moving frame and one can construct the time-mean structure in this moving frame of reference (Cai and van den Dool, 1991).

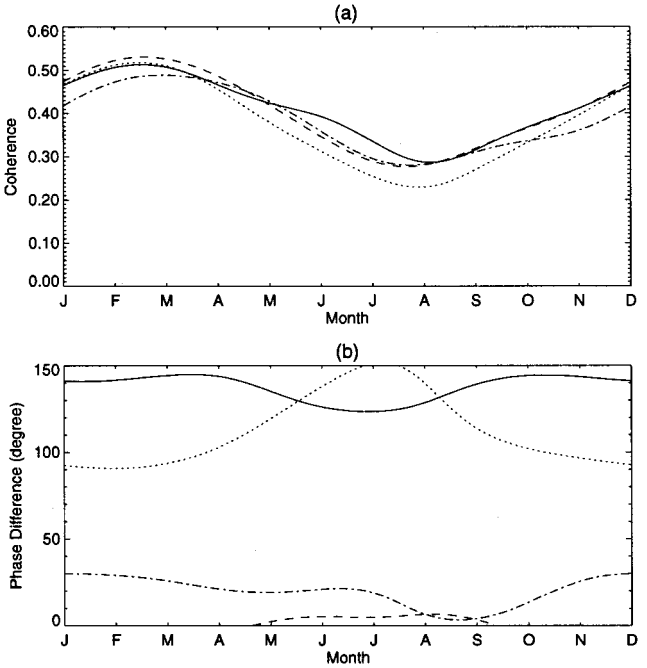

Figure 9. Seasonal variation of coherence squared and phase difference of eastward moving wave number one between 189 hPa zonal and meridional wind. Solid line for 2.2°N, short dash line for 20°N, long dash line for 33.3°N and dot dash line for 42°N

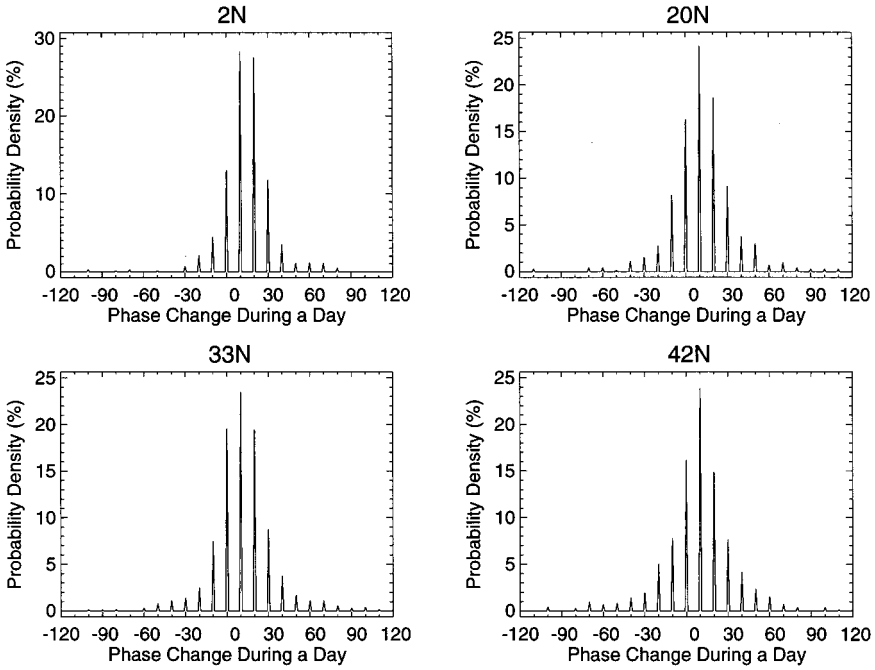

Figure 10. Histogram of the phase change during a day of the wave one for 189 hPa zonal wind in perpetual simulation at (a) 2.2°N; (b) 20°N; (c) 33.3°N; (d) 42°N. A positive (negative) phase change means an eastward (westward) propagation of the wave

The phase shifted structure for a flow variable S at the pressure level p, latitude ϕ and time t is defined as

$$\hat{S}(\lambda, \phi, p) = \frac{1}{T} \sum_{t=1}^{T} \{S(\lambda - \lambda^*, \phi, p, t) - [\overline{S(\phi, p)}]\}, \tag{10}$$

where λ is the longitude and λ^* is a shift in longitude which is a function of time and phase speed of the selected wave. $[\bar{S}]$ is the zonally averaged climatic mean field for S. The definition of λ^* is

$$\lambda^* = \frac{180}{\pi} \frac{KC_k(\phi_0)\,\Delta t}{a_e \cos(\phi_0)}, \tag{11}$$

where $C_k(\phi_0)$ is the phase speed of the selected wave with wave number K, at latitude γ_0, $\Delta t = t - t_0$ and a_e is the radius of the earth.

It is obvious that the transformation Equation (10) is no more than translating the whole flow at each time t eastward by an angle λ^*. Therefore, the relative position of the wave components at each time are exactly preserved under this transformation. The transformation Equation (10) is equivalent to following the selected wave in a moving frame with a speed equal to $C_k(\phi_0)$ so that the selected wave becomes stationary in the phase-shift flow.

Shown in Figure 12 are the composite structures of the vectors and the potential (contours) of the horizontal velocity field in the perpetual simulation for (a) 189 hPa, and (b) 787 hPa, as functions of latitude and relative longitude. The composite results are obtained by performing the phase-shift transformation, following a wave with eastward phase speed of 11.5 m/s in order to enhance the eastward-moving components, having a 40-day period in the perpetual simulation. The phase speed used here is determined by the eastward spectral peak of wave number one in the 189 hPa zonal wind (Figure 2(a)). The velocity potential pattern at 189 hPa is a minimum along the equator at 20° west of the middle axis. The maxima are displaced 180° from this minimum. An analogous composite at 778 hPa bears a strong resemblance to this pattern, except for a sign reversal. This composite is similar to that found in the GFDL simulation (Lau *et al.*, 1988), except for the divergence and convergence centered at 20° west.

At both 189 and 787 hPa, the wind field between 15°N and 15°S, is dominated by the zonal wind component, with strong divergence (convergence) in the upper troposphere and convergence (divergence) in lower troposphere. This composite structure near the equator is similar to the Kelvin wave pattern. Away from the equator, the composite exhibits Rossby wave vortices. This Kelvin-Rossby wave pattern was also simulated by Hayashi and Golder (1993) and Yip and North (1993).

Figure 13(a, b) are the composites of the 189 hPa horizontal velocity field in the seasonal simulation from December–January–February (DJF) and June–July–August (JJA). The composite structures in the seasonal simulation are obtained by following a wave with eastward phase speed of 9.5 m/s in order to enhance the eastward-moving components having a 50-day period. No velocity potential is drawn in Figure 13 because, unlike the perpetual simulation where the composite has a north–south symmetry, the intention here to is to compare the wind field in the winter hemisphere with that in the summer hemisphere. Comparing Figure 13 with Figure 12, the composite structure near the equator for both DJF and JJA are similar to that of the perpetual simulation. The wind field between 15°N and 15°S is dominated by the zonal wind component, with strong divergence of 0° in relative longitude. It implies that the low-frequency Kelvin wave has no obviously seasonal variation. But away from the equator, the Rossby wave seems strongly modulated by the seasonal cycle. The Rossby mode is much stronger in the winter hemisphere than in the summer one. It is reasonable since the baroclinic instability is stronger in winter. This result seems to suggest that the Rossby mode is one of the major components that are responsible for the seasonal variation. Hsu *et al.* (1990) suggested that some intraseasonal oscillations may be initiated by Rossby waves propagating from higher latitudes into equatorial regions.

5. CONCLUSIONS AND DISCUSSIONS

The spectral analysis of the intraseasonal oscillations in the 15-year perpetual and seasonal simulation, using NCAR CCM2 with zonally symmetric boundary conditions has been presented. The findings of the study can be summarized as follows:

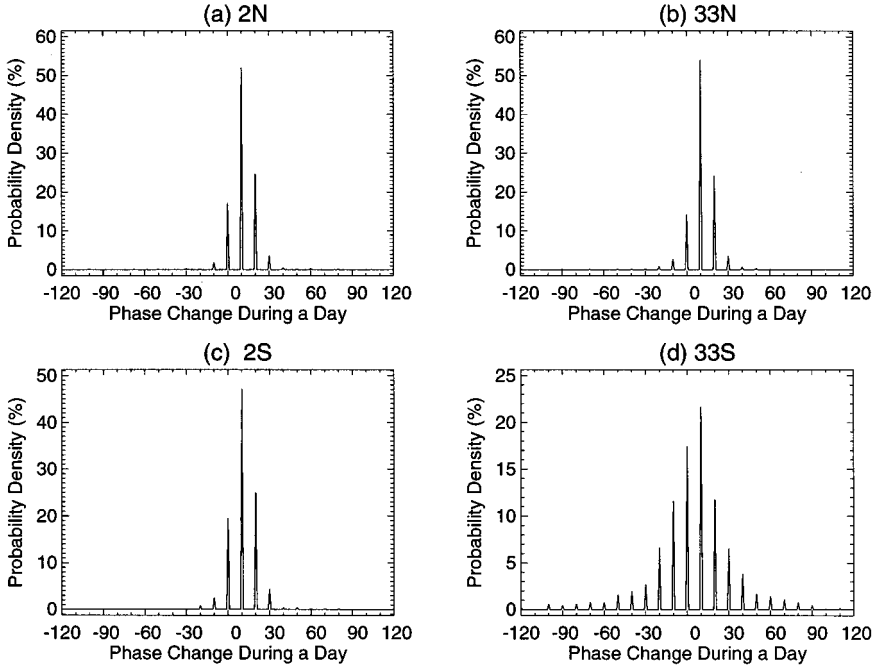

Figure 11. Histogram of the phase change during a day of the wave one for 189 hPa zonal wind during DJF in seasonal simulation at (a) 2.2°N; (b) 33.3°N; (c) 2.2°S; (d) 33.3°S. A positive (negative) phase change means an eastward (westward) propagation of the wave

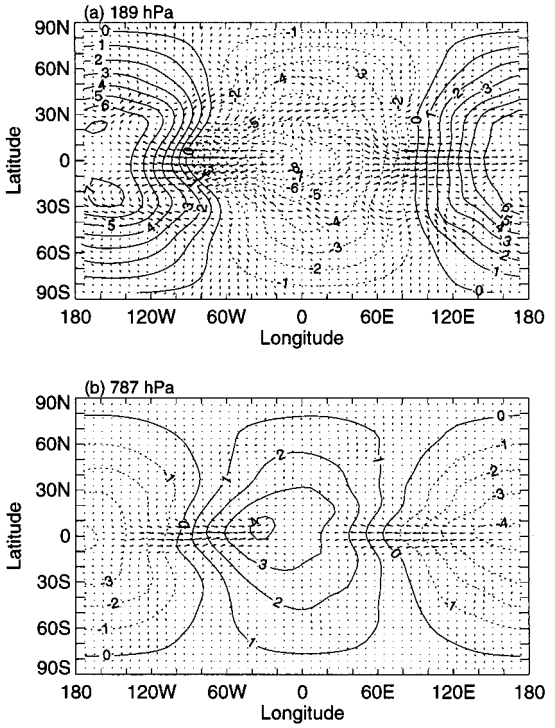

Figure 12. Longitude–latitude distribution of the eastward-moving composite fields of the velocity potential (contours) and horizontal wind vector (arrow) at (a) 189, and (b) 787 hPa following the low-frequency wave number one of 189 hPa zonal wind at 2.2°N. Contour interval is 1×106 m^2/s. The dashed line is for negative values

(i) the space–time spectra of zonal and meridional winds exhibit a well-defined 50-day period peak at eastward-moving wave number one in the seasonal simulation, while the period of oscillation is only 40 days in the perpetual simulation.

(ii) Cyclic spectral analysis of the seasonal simulation indicates that the intraseasonal oscillations are also localized according to time of year. The intraseasonal oscillations are stronger during winter than during summer.

(iii) The upper- and lower-level intraseasonal disturbances of zonal wind tend to be most coherent and out of phase near the equator. This might suggest that these disturbances have the structure of Kelvin waves at near-equatorial latitudes.

(iv) The zonal wind and meridional wind of the intraseasonal disturbances are coherent and out of phase in low latitudes and in phase in mid-latitudes. Maximum values of coherence are obtained during the winter and spring months when the spectra are highest, and minimum values occur in the summer, when the spectra are low.

(v) Statistics of phase variation show that the probability distribution of phase changes has an obvious seasonal variation, especially in mid-latitudes, where the probability distribution is narrow-centered, and of 40–50 days in period in the winter hemisphere, but it is broad in the summer hemisphere.

(vi) A phase shifting method has been used to construct the composite structure which exhibits Kelvin-Rossby wave patterns in both simulations. It is well known that the Rossby wave activities are dependent on season. The dependence of the oscillation on Rossby waves suggests that the activity of low-frequency Rossby waves could be one of the major factors that are responsible for the seasonal variation of intraseasonal oscillations.

These results demonstrate that there exists an intraseasonal oscillation even in the presence of highly symmetric surface boundary features and perpetual equinox solar distribution. The intraseasonal oscilla-

tions may be generated by the internal dynamics of the model, instead of being directly forced by imposed boundary conditions. However, intraseasonal oscillation may also be affected by the seasonal cycle through one or more seasonally-dependent energy sources. The seasonal forcing not only modulates, but also changes, the intensity of intraseasonal oscillation.

It has been suggested by previous investigators that the intraseasonal oscillations are associated with a horizontally coupled Rossby-Kelvin wave in the presence of large-scale moisture processes (Hayashi and Sumi 1986; Wang and Rui, 1990; Wang and Li, 1994). Seasonal variations in the generation of Rossby wave activity by baroclinic instability in mid-latitudes can produce variations in the flux of Rossby wave activity into the tropics and thus lead to variability in the vorticity field within the tropics. Such interaction between the tropics and extratropics might be partially responsible for the seasonal variation of the intraseasonal oscillations.

All of the above conclusions are model dependent. Many additional experiments need to be conducted in order to further test the possibilities advanced here, based on the CCM2/R15 simulation. It is necessary to ascertain if some of the simplifications applied to the model are crucial to drawing the main conclusions.

ACKNOWLEDGEMENTS

The authors would like to thank Dr. North for providing us with the CCM2 simulation data upon which this paper is based, and Dr. Yi for assistance in some data processing. The research was supported by research grants from the Canadian Natural Science and Engineering Research Council, the Atmospheric Environment Service of Canada.

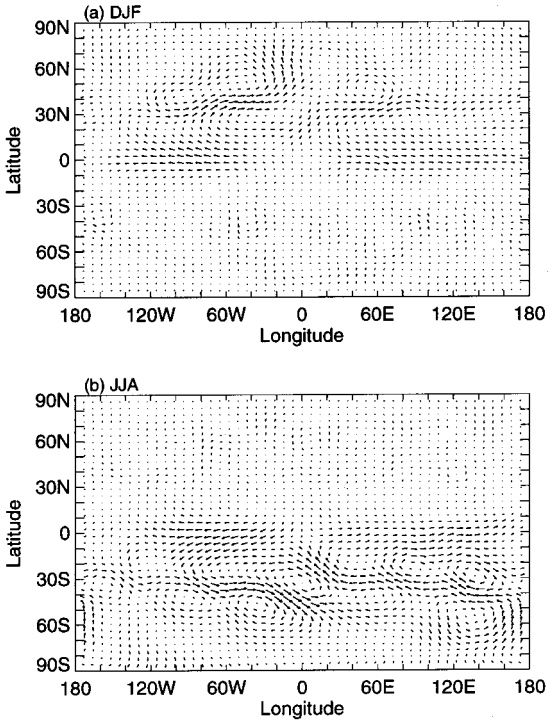

Figure 13. Longitude–latitude distribution of the eastward-moving composites field of the 189 hPa horizontal wind vector (arrow) of the seasonal simulation during (a) DJF; (b) JJA

REFERENCES

Anderson, J.R. and Rosen, R.D. 1983. 'The latitude-height structure of 40–50-day variation in atmospheric angular momentum', *J. Atmos. Sci.*, **40**, 1584–1591.

Cai, M. and van den Dool, H.M. 1991. 'Low-frequency waves and traveling storm track. Part I: barotropic component', *J. Atmos. Sci.*, **48,** 1420–1436.

Gardner, W.A. 1994. 'An introduction to cyclostationary signals', in Gardner, W.A. (ed.), *Cyclostationarity in Communications and Signal Processing*, IEEE Press, 1–90.

Gutzler, D.S. and Madden, R.A. 1993. 'Seasonal variations of the 40–50-day oscillation in atmospheric angular momentum', *J. Atmos. Sci.*, **50**, 850–860.

Hayashi, Y. 1982. 'Space–time spectral analysis and its application to atmospheric waves', *J. Meteorol. Soc. Jpn.*, **60**, 156–171.

Hayashi, Y. and Golder, D.G. 1986. 'Tropical 40–50- and 25–30-day oscillations appearing in realistic and idealized GFDL climate models and the ECMWF dataset', *J. Atmos. Sci.*, **50**, 464–494.

Hayashi, Y. and Golder, D.G. 1993. 'Tropical intraseasonal oscillations appearing in a GFDL general circulation model and FGGE data. Part I: Phase propagation', *J. Atmos. Sci.*, **31**, 3058–3067.

Hayashi, Y. and Sumi, A. 1986. 'The 30–40-day oscillations simulated in an ''aqua planet'' model', *J. Meteorol. Soc. Jpn*, **64**, 451–467.

Huang, J.-P. and North, G.R. 1996. 'Cyclic spectral analysis of fluctuations in a GCM simulation', *J. Atmos. Sci.*, **53**, 370–379.

Huang, J.-P., Cho, H.-R. and North, G.R. 1996. 'Applications of the cyclic spectral analysis to the surface temperature fluctuations in a stochastic climate model and a GCM simulation', *Atmosphere-Ocean*, **34**, 627–646.

Huang, J.-P., Higuchi, K. and Trivett, N.B.A. 1997. 'Multiresolution fourier transform and its application on analysis of CO_2 fluctuations over alert', *J. Meteorol. Soc. Jpn*, **75**, 701–715.

Hsu, H.-H., Hoskins, B.J. and Jin, F.-F. 1990. 'The 1985/86 intraseasonal oscillation and the role of the extratropics', *J. Atmos. Sci.*, **47**, 823–839.

Knutson, T.R. and Weickmann, K.M. 1987. '30–60-day atmospheric oscillations: composite life cycles of convection and circulation anomalies', *Mon. Wea. Rev.*, **115**, 1407–1436.

Lau, N.-C., Held, I. M. and Neelin, J.D. 1988. 'The Madden-Julian oscillation in an idealized general circulation model', *J. Atmos. Sci.*, **45**, 3810–3812.

Lau, N.-C. and Lau, K.-M. 1986. 'The structure and propagation of intraseasonal oscillations appearing in a GFDL general circulation model', *J. Atmos. Sci.*, **43**, 2023–2047.

Lau, K.-M. and Weng, H.Y. 1995. 'Climate signal detection using wavelet transform: how to make a time series sing', *Bull. Am. Meteorol. Soc.*, **76,** 2391–2402.

Madden, R.A. 1986. 'Seasonal variation of the 40–50-day oscillation in the tropics', *J. Atmos. Sci.*, **43**, 3138–3158.

Madden, R.D. and Julian, P. 1971. 'Detection of a 40–50-day oscillation in the general wind in the tropical Pacific', *J. Atmos. Sci.*, **28**, 702–708.

Madden, R.D. and Julian, P. 1972. 'Description of global scale circulation cells in the tropics with 40–50 day period', *J. Atmos. Sci.*, **29**, 1109–1123.

Pitcher, E.J. and Geisler, J.E. 1987. 'The 40- to 50-day oscillation in a perpetual January simulation with a general circulation model', *J. Geophys. Res.*, **92**, 11971–11978.

Wang, B. and Li, T. 1994. 'Convective interaction with boundary-layer dynamics in the development of a tropical intraseasonal system', *J. Atmos. Sci.*, **51**, 1386–1400.

Wang, B. and Rui, H. 1990. 'Synoptic climatology of transient tropical intraseasonal convection anomalies: 1975–1985', *Meteorol. Atmos. Phys.*, **44**, 43–61.

Yip, K.-J. and North, G.R. 1993. 'Tropical waves in a GCM with zonal symmetry', *J. Climate*, **6**, 1691–1702.

